ACS OMEGA

http://pubs.acs.org/journal/acsodf

Article

In Situ Assembling of Glass Microspheres and Bonding Force Analysis by the Ultraviolet–Near-Infrared Dual-Beam Optical Tweezer System

Hengjie Tang, Tetsuo Kishi,* and Tetsuji Yano

Cite This: *ACS Omega* 2021, 6, 11869–11877

Read Online

ACCESS | Metrics & More | Article Recommendations

ABSTRACT: Microresonators show great potential as interlayer routing solutions for multilayered three-dimensional (3D) photonic communication networks. New techniques are needed for the convenient and in situ manipulation and immobilization of glass microspheres into functional structures. Herein, near-infrared (NIR) and ultraviolet (UV) lasers were used as optical tweezers to precisely arrange silica microspheres and UV-initiated immobilization in a 3D space. The NIR laser was used to trap targeted microspheres, and the UV laser was focused to immobilize the trapped microspheres in 3-methacryloxypropyltrimethoxysilane (MOPS) in ∼6 s. Optical force spectroscopy was performed using the optical tweezers to measure individual bond strength. Next, functional triangular pedestals were designed to flexibly control the gap space for vertical router applications in 3D photonic networks. Thus, the designed UV–NIR dual-beam optical tweezer system can be used to assemble arbitrary functional 3D structures, making it a valuable tool for microfabrication, photonics, and optical communication applications.

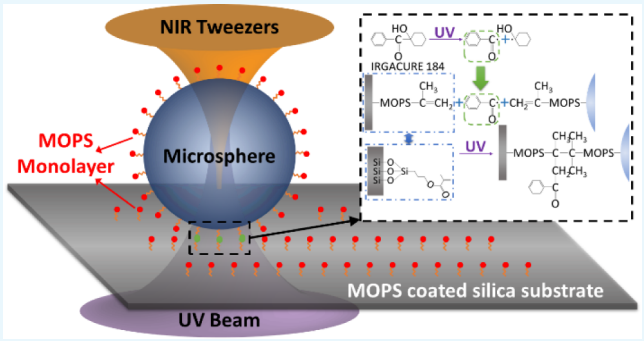

1. INTRODUCTION

Over the last several decades, photonic communication networks have emerged as the most promising approach to massively expand the bandwidth and reduce power consumption[1−4] relative to conventional metal-based electrical communication networks.[5−7] However, the increasing number of waveguide crossings causes optical loss and limits the scalability of the existing in-plane networks.[8−10] To resolve this issue, multilayered three-dimensional (3D) networks can provide efficient topologies and increase the density of integrated functional elements, which in conjunction can reduce energy requirements.[11−14]

Various components are integrated in a 3D photonic communication network, for example, modulators,[15,16] switches,[17,18] and filters.[19,20] The vertical router needed to establish interlayer links between stacked layers is the key component therein. Many solutions have been proposed for this router, such as microring vertical couplers,[21−23] vertical coupling waveguides,[24,25] and through-silicon photonic vias.[26] However, strict requirements for the vertical coupling distance and fabrication difficulties limit the applicability of these solutions. Recently developed chemical synthesis techniques have enabled the production of high-quality glass microspheres with controlled sizes, shapes, compositions, and other unique properties.[27−30] Functional devices constructed with glass microspheres find broad applications for photonics as ideal microresonator components with either active or passive compositions,[31−35] introducing new possibilities for vertical routers in 3D photonic networks.

The coupling behavior and quality factor of a microresonator integrated in a photonic network are precisely determined by the gap space between spheres and waveguides.[36] However, recent methods of coupling microspheres and controlling the gap are limited in terms of flexibility by predeposited Teflon films or the fiber taper,[36,37] which are incompatible with microfabrication requirements, particularly in 3D optical communication networks. New magnetic control methods have been reported,[38] but external fields and complex structures limit 3D-integrated applications. A new triangular pedestal structure (Figure 1) proposed herein can simply and flexibly control the gap to support microresonators on waveguides. The pedestal comprises several glass microspheres as vertices (named pedestal microspheres thereafter), and the

Received: January 7, 2021
Accepted: April 15, 2021
Published: April 27, 2021

https://doi.org/10.1021/acsomega.1c00109
ACS Omega 2021, 6, 11869–11877

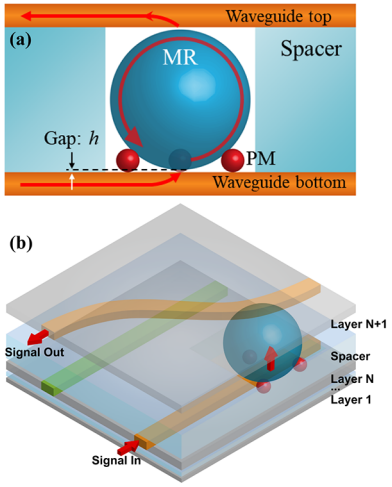

Figure 1. Schematic illustrations of (a) the triangular pedestal structure to control the gap space h and (b) an interlayer router model using microresonators and pedestals in a multilayered 3D photonic network. PM, pedestal microspheres; MR, microresonator.

structure can be flexibly adjusted to obtain the desired gap spaces.

Individual glass microspheres are assembled into a functional component in two steps: arrangement into the desired configuration in the first step and immobilization in the second step. Numerous techniques have been reported to perform each step separately.[39−47] However, simultaneously executing both steps remains challenging because microspheres generally become disorganized when the external field is removed prior to immobilization.[48,49] Efforts have been made to effectively combine the assembly and immobilization steps. Cascading microresonators on glass substrates coated with epoxy resin have also been reported, but immobilization in this case was uncontrollable once the microspheres touched the coated substrates.[50] Terray et al. used a laser to initiate polymerization in aqueous solution and created structures in situ; however, these structures were limited to a linear configuration along the trapping beam, which is particularly unsuitable for 3D construction.[51] Misawa et al. provided an in situ common path strategy, but the vinyl monomer solution still risked uncontrolled polymerization by scattered light.[52,53] UV-initiated click chemistry, an efficient alternative for in situ immobilization, is highly controllable and compatible with many manipulation techniques.[54,55] However, light-emitting diode illumination, commonly used to initiate click reactions, has poor targeting precision and long reaction times, rendering these methods impractical for industrial fabrication.[56−58] Thus, there remains a need for an efficient, convenient method for immobilizing targeted glass microspheres in situ following assembly.

Herein, a convenient UV−NIR dual-beam optical tweezer system was developed to precisely arrange glass microspheres and achieve accurate UV-initiated immobilization in 3D space within seconds. An NIR laser was used as a trapping beam for manipulation, and a 325 nm UV laser was trained on the same focal area to initiate immobilization. The glass microspheres and substrates were coated with a monolayer of methacryloxypropyltrimethoxysilane (MOPS) and bonded to each other via polymerization between two MOPS molecules. The UV immobilization parameters were quantitatively evaluated, including the irradiation time and reagent concentration. Optical force spectroscopy was performed using the optical tweezers to directly measure the bonding strength of MOPS chains at different MOPS concentrations. A flexible pedestal structure was designed and assembled to support vertical routers in multilayered photonics networks.

2. RESULTS

2.1. Manipulation Using the NIR Optical Tweezers.

We first analyzed the lateral force of the NIR optical tweezers. Silica microspheres were trapped between the cover and slide glass in ethanol and moved laterally using the optical tweezers to indirectly determine the lateral force. The resisting force of a viscous fluid (F_{res}) surrounding a moving microsphere is related to its velocity according to Stokes' law (eq 1):

$$F_{res} = 6\pi\eta r v \quad (1)$$

where η is the viscosity of the liquid, here ethanol; r is the radius of the microsphere; and v is the velocity of the microsphere relative to the surrounding liquid. The lateral force of the optical tweezers is equal to the resisting force at the critical escape velocity. Notably, the surface viscosity would vary with the bulk value, considering the surface modification and particle sizes. We used a sedimentation test in pure ethanol to confirm that the surface viscosity of unprocessed silica microspheres used therein showed no significant deviation

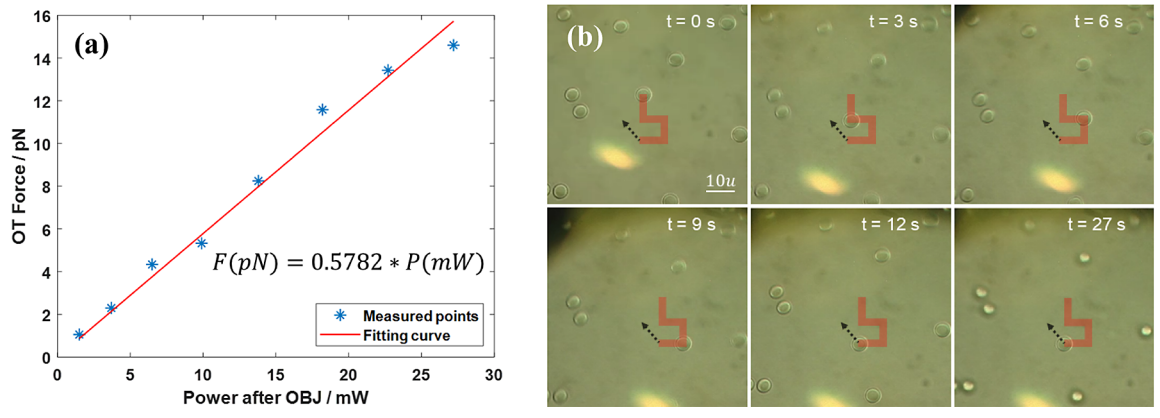

Figure 2. (a) Lateral force (pN) of the optical tweezers (OT) as a function of laser power (mW) (measured after the OBJ). The red line is the fitted curve. (b) Images showing the sequence in which a single silica microsphere was moved using the optical tweezer system. The red lines represent the lateral movement, and the black arrows represent the axial lift.

https://doi.org/10.1021/acsomega.1c00109
ACS Omega 2021, 6, 11869−11877

(<0.3%) from the bulk value, and we therefore ignored its influence during subsequent calculations.

The lateral force (F_{OT}) of the optical tweezers is plotted as a function of laser power (measured after the objective lens (OBJ)), as shown in Figure 2a. Up to 16 pN of force could be applied to the microspheres at a laser power of 30 mW. The optical tweezers could also be evaluated using the force coefficient (Q), which was calculated using eq 2.[59]

$$F_{OT} = Q\frac{n_1 P}{c} \quad (2)$$

where n_1 is the refractive index of the medium, P is the laser power, and c is the speed of light. The refractive index of ethanol, measured using an Abbe Refractometer (ATAGO), was 1.3610 (D line, 23 °C). Considering the solute concentration of the 3 wt % photoinitiator IRGACURE 184, the measured refractive index of the solution was 1.3650, and the influence on force was less than 0.32%; it is therefore ignored hereafter. After fitting the curve in Figure 2a, the maximum value of Q was found to be 0.1279. This implies that over 12% of the laser power was transferred and used to trap the target microsphere when the beam passed through it. Increasing the laser power would obviously increase the optical tweezer force, but the effects of heating, such as the generation of vortices in the heated liquid, should be considered.

We separately characterized manipulation in 3D space using the optical tweezers. One silica microsphere was trapped and moved along a predetermined path (Figure 2b). The coordinates of each node along the path were used as inputs for the control software. The piezo stage and the OBJ actuator were moved accordingly to manipulate the microsphere. The target microsphere was dragged 10 μm laterally and lifted 5 μm axially in 0.1 μm steps. The trapped microsphere was in focus, whereas the surrounding microspheres were out of focus. The speed of the microspheres could be precisely controlled below the critical escape velocity by adjusting the step size. However, the step size should not exceed the radius of the microsphere to avoid the risk of derailment. We were able to flexibly manipulate the microspheres in the 3D space and move them to any user-defined position, thus confirming that the developed UV−NIR dual-beam system can be used to generate complex 3D structures.

2.2. UV Immobilization. Once the microspheres were positioned using the optical tweezers, they were immobilized by the polymerization of MOPS chains formed during a UV-induced click reaction. MOPS is commercially available and widely used to fabricate hybrid sol−gel films for waveguides,[60,61] although few reports exist on the use of MOPS for particle immobilization. This rarity might be due in part to the long UV irradiation time required.[56−58] We focused the UV laser and optimized the MOPS concentration to shorten this irradiation time to a period of a few seconds; this shortening is important and efficient for practical applications such as industry fabrication.

MOPS was first hydrolyzed in an acidic environment, following which it could participate in a condensation reaction with the hydroxyl groups on the glass microspheres and slides. An MOPS monolayer coated the surface of each microsphere and the slide through the formation of siloxane (Si—O—Si) bonds (Figure 3). To control the polymerization reaction, we used a focused 325 nm UV laser as an external trigger for the photoinitiator. Photoinitiation induced polymerization bond formation between pairs of MOPS chains, linking the

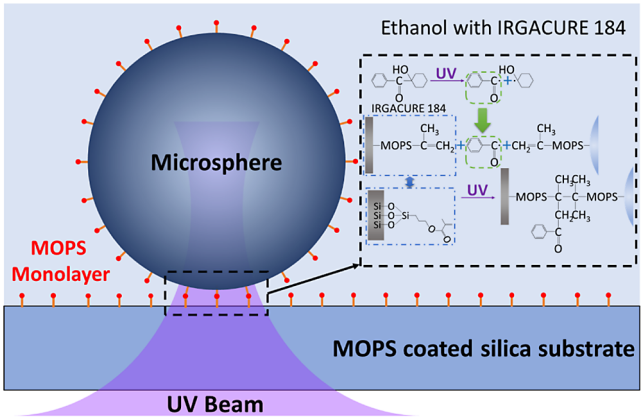

Figure 3. Schematic illustration of UV-initiated immobilization between the surfaces of microspheres and substrates coated with MOPS monolayers. The decomposition of the photoinitiator IRGACURE 184 under UV light initiated the bonding of adjacent MOPS chains. Inset: bonding process between MOPS chains.

microspheres to the glass substrate or to other microspheres, wherever the UV laser was focused. The reaction proceeded very quickly under the focused UV beam, ensuring that the operation of the optical tweezers would not be affected by immobilization, thus realizing an assembly line. Another benefit of focusing the UV laser was that immobilization exclusively occurred in targeted areas, resulting in excellent spatial precision.

The effect of MOPS concentration on UV immobilization was also investigated to optimize our protocol. The UV exposure times required to immobilize microspheres coated in MOPS at concentrations of 0.02−0.5 wt % are plotted, as shown in Figure 4a. Microspheres were observed in three different states following UV exposure (Figure 4b). Microspheres in the free state indicated that UV exposure was insufficient, and the trapped microspheres could still be moved using the optical tweezers. In the bound state, the microspheres were linked to the slide by some quantity of MOPS chains and could not be moved by applying a weak force (normally less than 5 pN). However, they could be disturbed or even dragged away if the optical tweezer force became stronger. More MOPS chains were found bonded to microspheres in the fixed state, and the microspheres could no longer be moved. We found that higher MOPS concentrations reduced the UV exposure time needed to efficiently immobilize individual microspheres, but they were saturated with MOPS at higher concentrations. This indicated that UV-induced immobilization was influenced by the density of the MOPS layer, which was governed by the concentration of the MOPS solution used to coat the microspheres and slides. When the MOPS coating on the surface was sparse, the likelihood of bonds forming between MOPS chains was lower. Coating with a 0.02 wt % MOPS solution resulted in longer and highly variable required UV exposure times. However, if the MOPS coating was too dense, the reaction rates at the center and edges of the irradiated area differed. This was due to the uneven distribution of the photoinitiator when MOPS reached saturation. The optimal MOPS concentration for coating the glass microspheres and slides was found to be 0.1 wt %. Immobilization was achieved within 6 s under a focused UV laser; this duration was nearly 2 orders of magnitude less

https://doi.org/10.1021/acsomega.1c00109
ACS Omega 2021, 6, 11869−11877

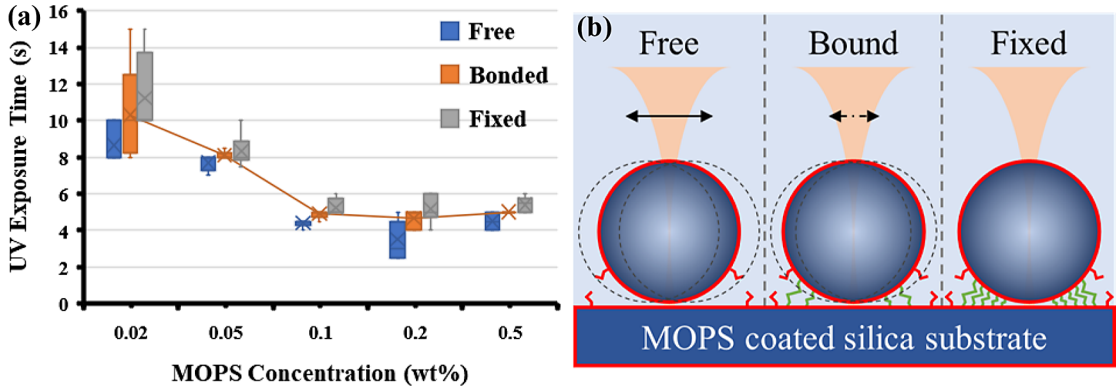

Figure 4. (a) Relationship between UV exposure time and MOPS concentration during the UV immobilization process. The exposure time needed to obtain the three immobilization states was statistically measured under NIR light at a power of 22 mW. X symbols show the average value for each condition, whereas the orange solid line shows the exposure time trend across MOPS concentration for all bonded states pooled. (b) Schematic illustration of microspheres in three immobilization states: the free state, in which a few MOPS chains are bonded; the bound state, in which a certain proportion of chains are bonded; and the fixed state, in which even more chains are bonded.

than typical MOPS illumination times of several minutes or even hours.[61]

We first attempt to manipulate and immobilize individual silica microspheres using our system as a proof-of-concept experiment. The optical microscope images of the two microspheres, which are moved to target positions and immobilized, are shown in Figure 5. The power of the optical

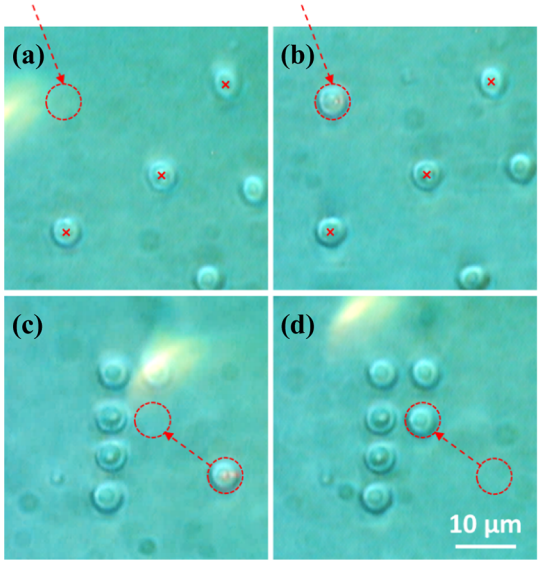

Figure 5. (a,c) *Ex ante* and (b,d) *ex post* optical microscope images showing the processes of manipulating two silica microspheres to target positions. The dashed circles and arrows represent the target microspheres and their motion path. The red X symbols in (a,b) indicate microspheres near the target positions, which serve as reference points.

tweezers was ~22 mW. This corresponded to ~12 pN of the optical tweezer force, which was sufficient to move the 5 μm microspheres. The UV laser was switched on and focused on the trapped microspheres to immobilize them. The power density behind the UV laser outlet was ~2.7 $\mu W/cm^2$. Manipulation and immobilization of the selected microspheres had no obvious impact on the surrounding microspheres, which was attributed to the targeting precision of the focused beam.

3. DISCUSSION

3.1. Bonding Strength. The optical tweezing force we applied was in the piconewton range, which enabled the evaluation of the MOPS chains' bonding strength using the optical tweezers in situ. The bonding force opposing the lateral force of the optical tweezers can be described using the simple lever model illustrated in Figure 6a, which shows a microsphere linked to a substrate by a pair of MOPS chains. The position of the fulcrum depends on where the MOPS bonds to the microsphere, until the chains break because of the optical tweezers. The bonding force (f_{bond}) can be derived from the optical tweezer lateral force (F_{OT}) using eq 3.

$$f_{bond} = \frac{F_{\perp}L_1}{L_2} = \frac{F_{OT}R\cos\theta}{y_F/\cos\theta} \tag{3}$$

where $F_{\perp}$ is the perpendicular component of F_{OT}; L_1 and L_2 are the lengths of the lever arms of the optical tweezers and bonding force, respectively; θ is the angle between the fulcrum and the normal axis; and y_F is the ordinate of the fulcrum, which is equal to the distance between the microsphere surface and the substrate. This exact distance depends on the area over which immobilization occurs, which primarily depends on the size of the UV focal area and the length of the bonded MOPS chains. y_F can be expressed using eq 4.

$$y_F = \min\begin{cases} R - \sqrt{R^2 - \mathrm{FWHM}_{UV}^2} \\ k \times \mathrm{CL}_{bonding} \end{cases} \tag{4}$$

where FWHM_{UV} is the full width at half-maximum of the UV focal profile, $\mathrm{CL}_{bonding}$ is the length of the bonded MOPS chains, and k is the structural folding factor of the MOPS molecule. The UV focal profile (I_{focal}) can be calculated using the Fraunhofer diffraction expression in eq 5.

$$I_{focal} = \mathrm{Fourier}\{I_{in} \times \mathrm{pupil}\} = I_{ideal} * \mathrm{PSF} \tag{5}$$

where PSF is the point spread function of the OBJ pupil. The length of the MOPS chains $\mathrm{CL}_{bonding}$ is determined from the sum of each chemical bond length, considering the bond angle.[62] The length of a single MOPS molecule, from the carbon participating in the photopolymerization reaction (asterisked) at one end —C*(CH_3)=CH_2 to the oxygen (asterisked) linked to surfaces at the other end —Si—O*—Si

https://doi.org/10.1021/acsomega.1c00109
ACS Omega 2021, 6, 11869−11877

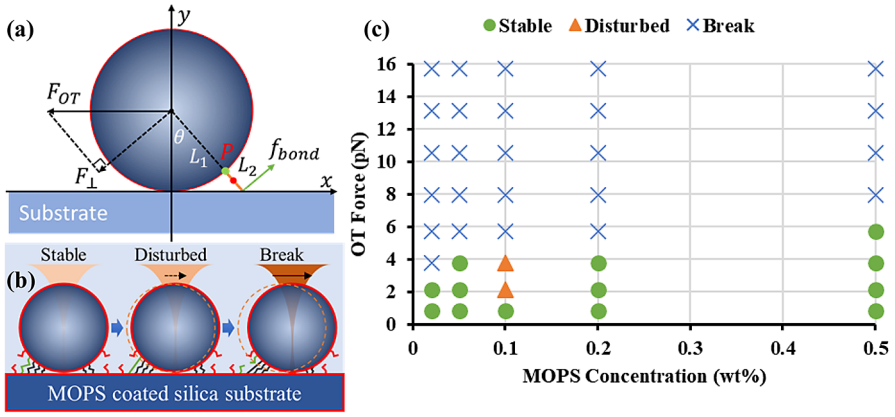

Figure 6. (a) Schematic illustration of the lever model, in which the bonding force f_{bond} opposes the lateral force F_{OT} of the optical tweezers. L_1 and L_2 are the lengths of the lever arms of F_{OT} and the bonding force, respectively; θ is the angle between the fulcrum and the normal axis; $F_\perp$ is the perpendicular component of F_{OT}; and P represents the fulcrum point. (b) Schematic illustration of the bond breakage process from the stable state to the disturbed state until breakage occurs with increasing F_{OT}. The outermost, tightest bonded chain (green) would break first when pulled by the optical tweezers before other chains broke one by one. The orange dashed circles represent the original position of the microsphere when stable. (c) Bonding strength, as evaluated with increasing optical tweezer force under various MOPS concentrations: 0.025, 0.05, 0.1, 0.2, and 0.5 wt %.

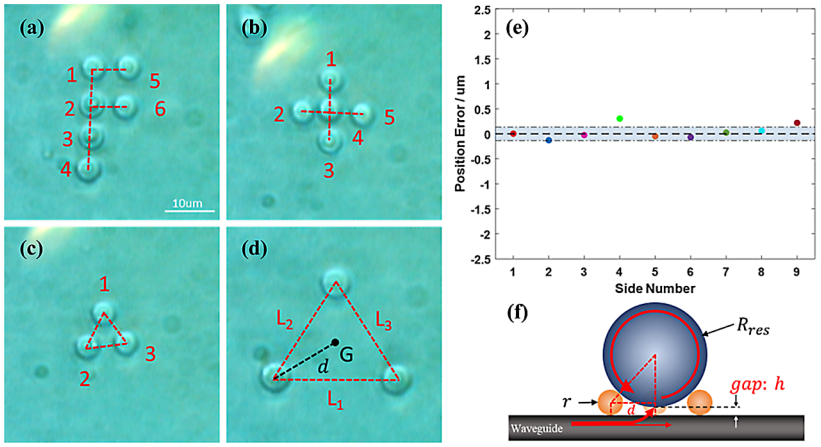

Figure 7. Optical images of microspheres manipulated into various patterns: (a) a letter "F" shape, (b) a cross, and (c) a triangle. (d) Pedestal structure comprising three pedestal microspheres arranged in an equilateral triangle. L is the length of each side, G is the center point, and d is the distance between the center and each vertex. (e) Distribution of the positional error determined by measuring all nine sides of the three triangles. The SD (0.14 μm) is indicated by blue shading. (f) Schematic illustration showing the adjustment of gap space h in a functional pedestal structure. R_{res} and r represent the radii of microresonators and pedestal microspheres, respectively, and d is the distance between the center and each vertex.

(shown in the inset of Figure 3), was calculated as 1.042 nm. The $CL_{bonding}$, comprising two bonded MOPS molecules, was double the length of a single MOPS molecule plus one C—C bond, resulting in a total length of 2.210 nm. Chains are normally folded; hence, k should be less than 1. For example, k was 0.5 where the MOPS chains overlapped. When the microsphere is pulled by the optical tweezers, the chains stretch and k approaches 1.

The microspheres in the bound state shown in Figure 4b could be dragged away when F_{OT} was sufficiently high. By carefully controlling the UV exposure time, we prepared several microspheres in the bound state, while varying F_{OT} by adjusting the NIR laser power. The microspheres were stable when weak F_{OT} was applied. Then, they were disturbed as the F_{OT} was increased and could be dragged away from the substrate when F_{OT} exceeded the bonding force and broke the chains (Figure 6b). The bonding strength of a single chain could be evaluated at the point of bond breakage (F_{OT} exceeding critical value) because the tightest bonded chain would break first when pulled by the optical tweezers before other chains broke one by one. The measured magnitudes of F_{OT} required to break bonds between the substrates and microspheres coated at different MOPS concentrations are shown in Figure 6c. Chains broke when F_{OT} exceeded 4−6 pN, and no significant relationship existed between F_{OT} and the MOPS concentration. The bonding force could then be calculated for a single chain using eq 3. The value of f_{bond} was 4.5 nN, which exactly matched the mechanical strength of covalent bonds in MOPS.[63,64] The Si—C bonds were considered more likely to break first, as they were the weakest bonds in the MOPS chains.[65]

3.2. Structural Assembly and Accuracy. To confirm that the UV−NIR dual-beam optical tweezer system can be used as a micromanufacturing tool for the precise construction of arbitrary functional structures, evaluating its structural assembly performance and accuracy was necessary. We organized microspheres into simple triangles, cross patterns, and letter "F" shapes by manipulating them to the target positions and immobilizing them individually (Figure 7).

https://doi.org/10.1021/acsomega.1c00109
ACS Omega 2021, 6, 11869−11877

The coupling behavior of a microresonator integrated with an optical waveguide in a photonic network is the most important design parameter as a determinant of the quality factor, stored energy, and bandwidth. Coupling behavior entirely depends on the gap space between the spheres and the waveguide; hence, flexible control over device morphology during fabrication is imperative.[36] We designed a functional pedestal structure (Figure 7d) as part of a flexible vertical router for interlayer communication in multilayered 3D photonic networks. The pedestal structure comprised three pedestal microspheres, which were organized into an equilateral triangle to support a large microresonator (Figure 1a). By properly adjusting the locations of the three vertices, the gap space between the resonator and the waveguide (h) could be precisely controlled using eq 6.

$$h = \sqrt{(R_{res} + r)^2 - d^2} + r - R_{res} \quad (6)$$

where R_{res} and r are the radii of the microresonator and pedestal microspheres at the vertices, respectively, and d is the distance between each vertex and the center of the triangle. In Table 1, we list some examples with various resonators and pedestal microsphere size combinations to design pedestals for three representative communication wavelengths (h was set equal to one-quarter of the applicable wavelength).[66]

Table 1. Pedestal Design Parameters for Three Representative Communication Wavelengths

λ/μm	h	r	R_{res}	d
1.55	0.39	5.0	100.0	43.9
1.55	0.39	5.0	50.0	31.1
1.30	0.33	2.0	100.0	27.1
1.30	0.33	2.0	50.0	19.2
0.85	0.21	1.0	100.0	18.9
0.85	0.21	1.0	50.0	13.4

To assess accuracy, we arranged three microspheres to predetermined coordinates to form each pedestal structure and immobilized them. We repeated the process thrice and captured optical images to measure all nine sides of the pedestals. The positional error was calculated for each side, which was defined as the difference between the theoretical and measured lengths. The measured lengths of all nine sides were remarkably close to their expected values with a standard deviation (SD) of 0.14 μm (Figure 7e). The SD was less than 1/30th of the silica microsphere diameter, and the corresponding error in h in the first line of Table 1 was just 60 nm according to eq 6. The accurate assembly of structures at the submicron level confirmed that the optical tweezer system can be used for precise microdevice fabrication.

4. CONCLUSIONS

A custom UV−NIR dual-beam system was developed for the manipulation and assembly of glass microspheres into compact functional structures by combining optical tweezers with a UV immobilization strategy. Up to 16 pN of the optical tweezer lateral force could be applied to the microspheres at laser powers below 30 mW, and the force coefficient (Q) exceeded 0.12. The effect of the MOPS concentration used to coat the glass microspheres and substrates was evaluated, and an MOPS concentration of 0.1 wt % afforded rapid and reliable UV-induced immobilization. After optimizing the MOPS coating process and focusing the UV beam, UV-induced immobilization could be achieved within 6 s. This irradiation time was shorter than typical irradiation times by nearly 2 orders of magnitude. The bonding strength of individual MOPS chains was quantified via optical force spectroscopy using the optical tweezers. Each individual MOPS chain could supply 4−6 pN bonding force for immobilization. The system was used to organize glass microspheres into various structures with submicron accuracy. We constructed a pedestal structure as a component of a vertical coupler. The distance between the microresonator and waveguide could be controlled to flexibly modulate the coupling behavior and the quality factor for interlayer communication in 3D photonic networks.

Additional research is needed to increase the flexibility of the manipulation and improve control over particle orientation, particularly the orientations of irregular particles. The modulation of the trapping beam wave front could induce vortex torque in the focal area.[67,68] Although our system enabled the manipulation of individual microspheres, throughput was relatively low, which can constitute a barrier against use in integrated manufacturing applications. However, using a galvanometer or a programmatically controlled spatial light modulator[69−71] would enable parallel implementation of trapping and immobilization. We thus achieved the dynamic assembly of glass microspheres into 3D functional components for microdevices, providing our developed optical tweezer system to be a noninvasive and accurate tool for various micromanufacturing and 3D photonic network applications in optical communication.

5. MATERIALS AND METHODS

5.1. System Configuration. Our customized system was built based on an inverted microscope (Nikon, Japan), as shown in Figure 8. A 3900S tunable, continuous-wave (CW) Ti:sapphire NIR laser (Spectra-Physics, USA) served as the trapping beam. A half-wave plate (HWP), a polarized beam splitter (PBS), and an alternative neutral density filter were

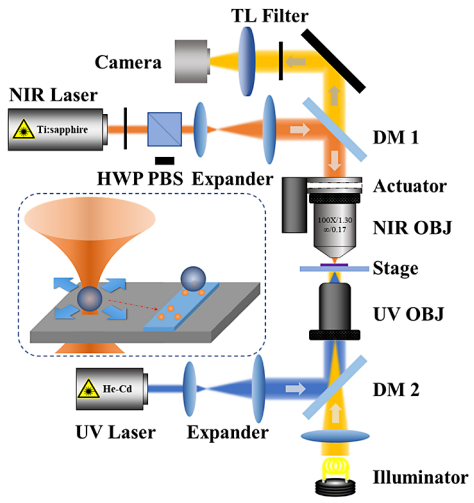

Figure 8. Schematic of the UV−NIR dual-beam optical tweezer system. The NIR beam was modulated by an HWP with a PBS and was directed to the NIR OBJ by a dichroic mirror (DM1). The UV beam was directed to the UV OBJ by another dichroic mirror (DM2). The transmitted light was imaged by a CCD camera through a tube lens (TL) and a filter. Inset: schematic illustration of the structure assembly in the sample plane.

https://doi.org/10.1021/acsomega.1c00109
ACS Omega 2021, 6, 11869−11877

used to modulate laser power. A low-pass dichroic mirror (DM1) directed the expanded beam to a 100× NIR OBJ (NA 1.30, Nikon) to form an optical gradient for trapping. The transmitted light was directed to a camera for imaging. The beam from an IK5551R-F 325 nm UV laser (Kimmon Koha, Japan) was combined with the illuminator light using a high-pass dichroic mirror (DM2) and a 20× UV OBJ (Thorlabs, USA). The reflected UV beam and trapping beam were confocal in the sample plane. The sample was placed on an XY piezo stage (PI, Germany) with an OBJ actuator coupled to the NIR OBJ to move the targets within a 100 × 100 × 80 μm^3 space. The path and speed of movement could be preset and monitored in our customized software programmed in LabVIEW (National Instruments, USA).

5.2. Preparation of the Silica Microspheres and Slides. Silica microspheres (5 μm, Sekisui Chemical, Japan) and 25 × 25 × 0.5 mm silica slides (Daico MFG, Japan) were coated with MOPS (Shin-Etsu, Japan) monolayers via siloxane (Si—O—Si) bond formation (Scheme 1). The silica slides and microspheres were placed in boiling deionized (DI) water to activate the hydroxyl groups on their surfaces. They were then treated for 2 h in a solution containing MOPS in one of a set of concentrations (0.02, 0.05, 0.1, 0.2, and 0.5 wt %) and 5 wt % HCl in ethanol, which had been stirred for 2 h in advance. The coated slides were then washed with ethanol and dried under nitrogen. The coated microspheres were washed and centrifuged twice in ethanol to remove excess MOPS and were subsequently collected and suspended in ethanol. The mixtures were ultrasonicated for 10 min for dispersion. Prior to the placement on the XY piezo stage, 3 wt % IRGACURE 184 (1-hydroxycyclohexyl-phenylketone, BASF, Japan) was added to each suspension as the photoinitiator. The effect of photoinitiator concentration was evaluated, and the UV exposure time was found to reach a threshold when an IRGACURE 184 concentration exceeding 3 wt % was used. A 30 μm thick shim ring spacer was placed on each coated slide. The desired volume of the coated microsphere suspension was injected into the sample case and then sealed with a glass coverslip.

Scheme 1. Flowchart of the Process Used To Coat Silica Microspheres and Slides with MOPS Monolayers

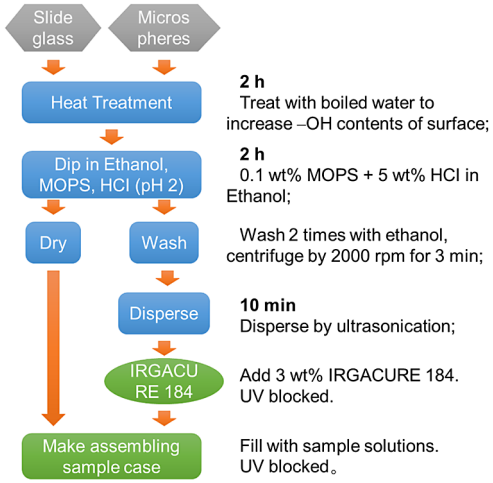

AUTHOR INFORMATION

Corresponding Author

Tetsuo Kishi − *Department of Material Science and Engineering, Tokyo Institute of Technology, Tokyo, Meguro-ku 145-0065, Japan;* orcid.org/0000-0002-8392-1360; Phone: +81-3-5734-2523; Email: tkishi@ceram.titech.ac.jp

Authors

Hengjie Tang − *Department of Material Science and Engineering, Tokyo Institute of Technology, Tokyo, Meguro-ku 145-0065, Japan;* orcid.org/0000-0003-1422-3785

Tetsuji Yano − *Department of Material Science and Engineering, Tokyo Institute of Technology, Tokyo, Meguro-ku 145-0065, Japan*

Complete contact information is available at: https://pubs.acs.org/10.1021/acsomega.1c00109

Notes

The authors declare no competing financial interest.

ACKNOWLEDGMENTS

This work was financially supported by the Iketani Science and Technology Foundation (ISTF).

ABBREVIATIONS

UV	ultraviolet
NIR	near-infrared
DM	dichroic mirror
CW	continuous wave
HWP	half-wave plate
PBS	polarized beam splitter
TL	tube lens
OBJ	objective lens
DI	deionized
FWHM	full width at half-maximum
PSF	point spread function
SD	standard deviation

REFERENCES

(1) Shacham, A.; Bergman, K.; Carloni, L. P. Photonic Networks-on-Chip for Future Generations of Chip Multiprocessors. *IEEE Trans. Comput.* **2008**, *57*, 1246−1260.

(2) Parini, A.; Ramini, L.; Lanzoni, F.; Bellanca, G.; Bertozzi, D. Bottom-Up Abstract Modelling of Optical Networks-on-Chip: From Physical to Architectural Layer. *Int. J. Opt.* **2012**, *2012*, No. 902849.

(3) Calò, G.; Petruzzelli, V. Generic Wavelength-Routed Optical Router (GWOR) Based on Grating-Assisted Vertical Couplers for Multilayer Optical Networks. *Opt. Commun.* **2016**, *366*, 99−106.

(4) Calò, G.; Petruzzelli, V. Grating-Assisted Vertical Couplers for Signal Routing in Multilayer Integrated Optical Networks. *Opt. Commun.* **2017**, *386*, 6−13.

(5) Briere, M.; Girodias, B.; Bouchebaba, Y.; Nicolescu, G.; Mieyeville, F.; Gaffiot, F.; O'Connor, I. System Level Assessment of an Optical NoC in an MPSoC Platform. *2007 Design, Automation Test in Europe Conference Exhibition*, Nice, France, 2007, pp 1−6. DOI: DOI: 10.1109/DATE.2007.364438

(6) Miller, D. A. B. Device Requirements for Optical Interconnects to Silicon Chips. *Proc. IEEE* **2009**, *97*, 1166−1185.

(7) Li, C. T.; Zheng, C. T.; Zheng, Y.; Huang, X. L.; Zhang, D. M.; Ma, C. S. Topology and Investigation of a Polymer 8-Port Optical Router with Scalable 7N Channel Wavelengths Using N-Stage Cascading Structure. *Opt. Commun.* **2015**, *339*, 94−107.

(8) Batten, C.; Joshi, A.; Orcutt, J.; Khilo, A.; Moss, B.; Holzwarth, C. W.; Popovic, M. A.; Li, H.; Smith, H. I.; Hoyt, J. L.; Kartner, F. X.; Ram, R. J.; Stojanovic, V.; Asanovic, K. Building Many-Core Processor-to-DRAM Networks with Monolithic CMOS Silicon Photonics. *IEEE Micro* **2009**, *29*, 8−21.
(9) Morris, R.; Kodi, A. K.; Louri, A. Dynamic Reconfiguration of 3D Photonic Networks-on-Chip for Maximizing Performance and Improving Fault Tolerance. *2012 45th Annual IEEE/ACM International Symposium on Microarchitecture*, Vancouver, BC, Canada; IEEE, 2012, pp 282−293. DOI: DOI: 10.1109/MICRO.2012.34
(10) Guo, P.; Hou, W.; Guo, L.; Zhang, X.; Ning, Z.; Obaidat, M. S. Design for Architecture and Router of 3D Free-Space Optical Network-on-Chip. *IEEE Int. Conf. Commun.* **2018**, DOI: 10.1109/ICC.2018.8422790.
(11) Chen, K. X.; Chu, P. L.; Chiang, K. S.; Chan, H. P. Design and Fabrication of a Broadband Polymer Vertically Coupled Optical Switch. *J. Light. Technol.* **2006**, *24*, 904−910.
(12) Koonath, P.; Jalali, B. Multilayer 3-D Photonics in Silicon. *Opt. Express* **2007**, *15*, 12686−12691.
(13) Preston, K.; Manipatruni, S.; Gondarenko, A.; Poitras, C. B.; Lipson, M. Deposited Silicon High-Speed Integrated Electro-Optic Modulator. *Opt. Express* **2009**, *17*, 5118−5124.
(14) Agrawal, M.; Chakrabarty, K.; Widialaksono, R. Reuse-Based Optimization for Prebond and Post-Bond Testing of 3-D-Stacked ICs. *IEEE Trans. Comput. Des. Integr. Circuits Syst.* **2015**, *34*, 122−135.
(15) Xu, Q.; Manipatruni, S.; Schmidt, B.; Shakya, J.; Lipson, M. 12.5 Gbit/s Carrier-Injection-Based Silicon Micro-Ring Silicon Modulators. *Opt. Express* **2007**, *15*, 430−436.
(16) Thomson, D. J.; Gardes, F. Y.; Hu, Y.; Mashanovich, G.; Fournier, M.; Grosse, P.; Fedeli, J.-M.; Reed, G. T. High Contrast 40Gbit/s Optical Modulation in Silicon. *Opt. Express* **2011**, *19*, 11507−11516.
(17) Van Campenhout, J.; Green, W. M. J.; Vlasov, Y. A. Design of a Digital, Ultra-Broadband Electro-Optic Switch for Reconfigurable Optical Networks-on-Chip. *Opt. Express* **2009**, *17*, 23793−23808.
(18) Xie, N.; Hashimoto, T.; Utaka, K. Design and Performance of Low-Power, High-Speed, Polarization-Independent and Wideband Polymer Buried-Channel Waveguide Thermo-Optic Switches. *J. Light. Technol.* **2014**, *32*, 3067−3073.
(19) Calò, G.; D'Orazio, A.; Grande, M.; Marrocco, V.; Petruzzelli, V. Active InGaAsP/InP Photonic Bandgap Waveguides for Wavelength-Selective Switching. *IEEE J. Quantum Electron.* **2011**, *47*, 172−181.
(20) Zhang, D.; Li, X.; Huang, X.; Liu, S.; Fu, H.; Che, K.; Wang, L. Optical Amplification at 1064 Nm in Nd(TTA) 3(TPPO) 2 Complex Doped SU-8 Polymer Waveguide. *IEEE Photonics J.* **2015**, *7*, 1−7.
(21) Huang, Y.; Paloczi, G. T.; Poon, J. K. S.; Yariv, A. Bottom-up Soft-Lithographic Fabrication of Three-Dimensional Multilayer Polymer Integrated Optical Microdevices. *Appl. Phys. Lett.* **2004**, *85*, 3005−3007.
(22) Lu, Z. Efficient Fiber-to-Waveguide Coupling through the Vertical Leakage from a Microring. *Opt. Lett.* **2007**, *32*, 2861−2863.
(23) Guo, P.; Hou, W.; Guo, L.; Yang, Q.; Ge, Y.; Liang, H. Low Insertion Loss and Non-Blocking Microring-Based Optical Router for 3D Optical Network-on-Chip. *IEEE Photonics J.* **2018**, *10*, 1−10.
(24) Parini, A.; Calò, G.; Bellanca, G.; Petruzzelli, V. Vertical Link Solutions for Multilayer Optical-Networks-on-Chip Topologies. *Opt. Quantum Electron.* **2014**, *46*, 385−396.
(25) Jiang, M.; Zhang, D.; Lian, T.; Wang, L.; Niu, D.; Chen, C.; Li, Z.; Wang, X. On-Chip Integrated Optical Switch Based on Polymer Waveguides. *Opt. Mater. (Amst)* **2019**, *97*, No. 109386.
(26) Guo, P.; Hou, W.; Guo, L.; Sun, W.; Liu, C.; Bao, H.; Duong, L. H. K.; Liu, W. Fault-Tolerant Routing Mechanism in 3D Optical Network-on-Chip Based on Node Reuse. *IEEE Trans. Parallel Distrib. Syst.* **2020**, *31*, 547−564.
(27) He, G.; Li, Y.; Bu, C.; Liu, G.; Jiang, W.; Li, J. Preparation of Ce-Doped (Y,Gd)3Al5O12 Nanoceramics by Sintering and Crystallization of Glass Microspheres. *Mater. Res. Bull.* **2015**, *66*, 45−50.
(28) Ghosh Dastidar, D.; Saha, S.; Chowdhury, M. Porous Microspheres: Synthesis, Characterisation and Applications in Pharmaceutical & Medical Fields. *Int. J. Pharm.* **2018**, *548*, 34−48.
(29) Xu, M.; Jin, C.; Jiang, Y.; Zhang, H. Preparation and Characterization of Functional Microspheres with Silicone. *Mater. Lett.* **2018**, *220*, 194−196.
(30) Soler-Carracedo, K.; Ruiz, A.; Martín, I. R.; Lahoz, F. Luminescence Whispering Gallery Modes in Ho^{3+} Doped Microresonator Glasses for Temperature Sensing. *J. Alloys Compd.* **2019**, *777*, 198−203.
(31) Lee, J. Y.; Hong, B. H.; Kim, W. Y.; Min, S. K.; Kim, Y.; Jouravlev, M. V.; Bose, R.; Kim, K. S.; Hwang, I. C.; Kaufman, L. J.; Wong, C. W.; Kim, P.; Kim, K. S. Near-Field Focusing and Magnification through Self-Assembled Nanoscale Spherical Lenses. *Nature* **2009**, *460*, 498−501.
(32) Paek, J.; Kim, J. Microsphere-Assisted Fabrication of High Aspect-Ratio Elastomeric Micropillars and Waveguides. *Nat. Commun.* **2014**, *5*, No. 3324.
(33) Huszka, G.; Gijs, M. A. M. Turning a Normal Microscope into a Super-Resolution Instrument Using a Scanning Microlens Array. *Sci. Rep.* **2018**, *8*, No. 601.
(34) Fernandez-Bravo, A.; Yao, K.; Barnard, E. S.; Borys, N. J.; Levy, E. S.; Tian, B.; Tajon, C. A.; Moretti, L.; Altoe, M. V.; Aloni, S.; Beketayev, K.; Scotognella, F.; Cohen, B. E.; Chan, E. M.; Schuck, P. J. Continuous-Wave Upconverting Nanoparticle Microlasers. *Nat. Nanotechnol.* **2018**, *13*, 572−577.
(35) Wang, M.; Jin, X.; Li, F.; Cai, B.; Yang, Y.; Zeng, S.; Wang, K. Label-Free Nanoparticle Sensors Based on a Triple-Layer-Coated Microsphere Structure. *Mater. Lett.* **2019**, *244*, 211−214.
(36) Panitchob, Y.; Murugan, G. S.; Zervas, M. N.; Horak, P.; Berneschi, S.; Pelli, S.; Nunzi Conti, G.; Wilkinson, J. S. Whispering Gallery Mode Spectra of Channel Waveguide Coupled Microspheres. *Opt. Express* **2008**, *16*, No. 11066.
(37) Senthil Murugan, G.; Panitchob, Y.; Tull, E. J.; Bartlett, P. N.; Hewak, D. W.; Zervas, M. N.; Wilkinson, J. S. Position-Dependent Coupling between a Channel Waveguide and a Distorted Microsphere Resonator. *J. Appl. Phys.* **2010**, *107*, No. 053105.
(38) Xia, J.; Qiao, Q.; Zhou, G. Controllable Gap in Microsphere Resonator Integrated with a Deformable Ferrofluid Droplet for Magnetic Field Sensing. *Opt. Fiber Technol.* **2020**, *58*, No. 102292.
(39) Zhu, J.; Li, M.; Rogers, R.; Meyer, W.; Ottewill, R. H.; Russel, W. B.; Chaikin, P. M.; STS-73 Space Shuttle Crew. Crystallization of Hard-Sphere Colloids in Microgravity. *Nature* **1997**, *387*, 883−885.
(40) Veen, S. J.; Antoniuk, O.; Weber, B.; Potenza, M. A. C.; Mazzoni, S.; Schall, P.; Wegdam, G. H. Colloidal Aggregation in Microgravity by Critical Casimir Forces. *Phys. Rev. Lett.* **2012**, *109*, No. 248302.
(41) Khanh, N. N.; Yoon, K. B. Facile Organization of Colloidal Particles into Large, Perfect One- and Two-Dimensional Arrays by Dry Manual Assembly on Patterned Substrates. *J. Am. Chem. Soc.* **2009**, *131*, 14228−14230.
(42) Retsch, M.; Jonas, U. Hierarchically Structured, Double-Periodic Inverse Composite Opals. *Adv. Funct. Mater.* **2013**, *23*, 5381−5389.
(43) Lumsdon, S. O.; Kaler, E. W.; Velev, O. D. Two-Dimensional Crystallization of Microspheres by a Coplanar AC Electric Field. *Langmuir* **2004**, *20*, 2108−2116.
(44) Yellen, B. B.; Hovorka, O.; Friedman, G. Arranging Matter by Magnetic Nanoparticle Assemblers. *Proc. Natl. Acad. Sci. U. S. A.* **2005**, *102*, 8860−8864.
(45) Yang, Y.; Pham, A. T.; Cruz, D.; Reyes, C.; Wiley, B. J.; Lopez, G. P.; Yellen, B. B. Assembly of Colloidal Molecules, Polymers, and Crystals in Acoustic and Magnetic Fields. *Adv. Mater.* **2015**, *27*, 4725−4731.
(46) Hayward, R. C.; Saville, D. A.; Aksay, I. A. Electrophoretic Assembly of Colloidal Crystals with Optically Tunable Micropatterns. *Nature* **2000**, *404*, 56−59.

(47) Dawood, F.; Qin, S.; Li, L.; Lin, E. Y.; Fourkas, J. T. Simultaneous Microscale Optical Manipulation, Fabrication and Immobilisation in Aqueous Media. *Chem. Sci.* **2012**, *3*, 2449−2456.
(48) Velev, O. D.; Gupta, S. Materials Fabricated by Micro- and Nanoparticle Assembly—The Challenging Path from Science to Engineering. *Adv. Mater.* **2009**, *21*, 1897−1905.
(49) Vogel, N.; Retsch, M.; Fustin, C. A.; Del Campo, A.; Jonas, U. Advances in Colloidal Assembly: The Design of Structure and Hierarchy in Two and Three Dimensions. *Chem. Rev.* **2015**, *115*, 6265−6311.
(50) Li, Y.; Abolmaali, F.; Allen, K. W.; Limberopoulos, N. I.; Urbas, A.; Rakovich, Y.; Maslov, A. V.; Astratov, V. N. Whispering Gallery Mode Hybridization in Photonic Molecules. *Laser Photonics Rev.* **2017**, *11*, No. 1600278.
(51) Terray, A.; Oakey, J.; Marr, D. W. M. Fabrication of Linear Colloidal Structures for Microfluidic Applications. *Appl. Phys. Lett.* **2002**, *81*, 1555−1557.
(52) Sasaki, K.; Koshioka, M.; Misawa, H.; Kitamura, N.; Masuhara, H. Pattern Formation and Flow Control of Fine Particles by Laser-Scanning Micromanipulation. *Opt. Lett.* **1991**, *16*, 1463.
(53) Misawa, H.; Sasaki, K.; Koshioka, M.; Kitamura, N.; Masuhara, H. Laser Manipulation and Assembling of Polymer Latex Particles in Solution. *Macromolecules* **1993**, *26*, 282−286.
(54) Ito, S.; Tanaka, Y.; Yoshikawa, H.; Ishibashi, Y.; Miyasaka, H.; Masuhara, H. Confinement of Photopolymerization and Solidification with Radiation Pressure. *J. Am. Chem. Soc.* **2011**, *133*, 14472−14475.
(55) Walker, D.; Singh, D. P.; Fischer, P. Capture of 2D Microparticle Arrays via a UV-Triggered Thiol-Yne "Click" Reaction. *Adv. Mater.* **2016**, *28*, 9846−9850.
(56) Fanizza, E.; Cozzoli, P. D.; Curri, M. L.; Striccoli, M.; Sardella, E.; Agostiano, A. UV-Light-Driven Immobilization of Surface-Functionalized Oxide Nanocrystals onto Silicon. *Adv. Funct. Mater.* **2007**, *17*, 201−211.
(57) Leem, G.; Zhang, S.; Jamison, A. C.; Galstyan, E.; Rusakova, I.; Lorenz, B.; Litvinov, D.; Lee, T. R. Light-Induced Covalent Immobilization of Monolayers of Magnetic Nanoparticles on Hydrogen-Terminated Silicon. *ACS Appl. Mater. Interfaces* **2010**, *2*, 2789−2796.
(58) Khatri, O. P.; Ichii, T.; Murase, K.; Sugimura, H. UV Induced Covalent Assembly of Gold Nanoparticles in Linear Patterns on Oxide Free Silicon Surface. *J. Mater. Chem.* **2012**, *22*, 16546−16551.
(59) Ashkin, A. Forces of a Single-Beam Gradient Laser Trap on a Dielectric Sphere in the Ray Optics Regime. *Methods Cell Biol.* **1998**, *61*, 1−27.
(60) Najafi, S. I.; Touam, T.; Sara, R.; Andrews, M. P.; Fardad, M. A. Sol-Gel Glass Waveguide and Grating on Silicon. *J. Light. Technol.* **1998**, *16*, 1640−1646.
(61) Zhang, X.; Lu, H.; Soutar, A. M.; Zeng, X. Thick UV-Patternable Hybrid Sol-Gel Films Prepared by Spin Coating. *J. Mater. Chem.* **2004**, *14*, 357−361.
(62) Wong, S. S.; Jameson, D. M. *Chemistry of Protein and Nucleic Acid Cross-Linking and Conjugation*, 2nd Edition; CRC Press, 2011. DOI: DOI: 10.1201/b11175
(63) Grandbois, M.; Beyer, M.; Rief, M.; Clausen-Schaumann, H.; Gaub, H. E. How Strong Is a Covalent Bond. *Science* **1999**, *283*, 1727−1730.
(64) Garnier, L.; Gauthier-Manuel, B.; Van Der Vegte, E. W.; Snijders, J.; Hadziioannou, G. Covalent Bond Force Profile and Cleavage in a Single Polymer Chain. *J. Chem. Phys.* **2000**, *113*, 2497−2503.
(65) Beyer, M. K. The Mechanical Strength of a Covalent Bond Calculated by Density Functional Theory. *J. Chem. Phys.* **2000**, *112*, 7307−7312.
(66) Nguyen, V. A.; Pham, V. D.; Hoang, T. H. C.; Le, H. T.; Hoang, T. T.; Ngo, Q. M.; Pham, V. H. A Quantitative Analysis of the Whispering-Gallery-Mode Lasers in Er3+-Doped Silica Glass Microspheres towards Integration in SOI Slotted Photonic Crystal Waveguides. *Opt. Commun.* **2019**, *440*, 14−20.
(67) Gahagan, K. T.; Swartzlander, G. A. Optical Vortex Trapping of Particles. *Opt. Lett.* **1996**, *21*, 827−829.
(68) Curtis, J. E.; Grier, D. G. Structure of Optical Vortices. *Phys. Rev. Lett.* **2003**, *90*, No. 133901.
(69) Chapin, S. C.; Germain, V.; Dufresne, E. R. Automated Trapping, Assembly, and Sorting with Holographic Optical Tweezers. *Opt. Express* **2006**, *14*, No. 13095.
(70) Min, T. L.; Mears, P. J.; Chubiz, L. M.; Rao, C. V.; Golding, I.; Chemla, Y. R. High-Resolution, Long-Term Characterization of Bacterial Motility Using Optical Tweezers. *Nat. Methods* **2009**, *6*, 831−835.
(71) Tanaka, Y. Double-Arm Optical Tweezer System for Precise and Dexterous Handling of Micro-Objects in 3D Workspace. *Opt. Lasers Eng.* **2018**, *111*, 65−70.

https://doi.org/10.1021/acsomega.1c00109
ACS Omega 2021, 6, 11869−11877